

# Spectroscopic factors for low-lying $^{16}\text{N}$ levels and the astrophysical $^{15}\text{N}(n, \gamma)^{16}\text{N}$ reaction rate

B. Guo,<sup>1,\*</sup> Z. H. Li,<sup>1</sup> Y. J. Li,<sup>1</sup> J. Su,<sup>1</sup> D. Y. Pang,<sup>2,3</sup> S. Q. Yan,<sup>1</sup> Z. D. Wu,<sup>1</sup> E. T. Li,<sup>4</sup> X. X. Bai,<sup>1</sup> X. C. Du,<sup>1</sup> Q. W. Fan,<sup>1</sup> L. Gan,<sup>1</sup> J. J. He,<sup>5</sup> S. J. Jin,<sup>1</sup> L. Jing,<sup>1</sup> L. Li,<sup>5</sup> Z. C. Li,<sup>1</sup> G. Lian,<sup>1</sup> J. C. Liu,<sup>1</sup> Y. P. Shen,<sup>1</sup> Y. B. Wang,<sup>1</sup> X. Q. Yu,<sup>5</sup> S. Zeng,<sup>1</sup> L. Y. Zhang,<sup>5</sup> W. J. Zhang,<sup>1</sup> and W. P. Liu<sup>1</sup>

*<sup>1</sup>China Institute of Atomic Energy,*

*P.O. Box 275(10), Beijing 102413, China*

*<sup>2</sup>School of Physics and Nuclear Energy Engineering,*

*Beihang University, Beijing 100191, China*

*<sup>3</sup>International Research Center for Nuclei and Particles in the Cosmos,*

*Beihang University, Beijing 100191, China*

*<sup>4</sup>College of Physics Science and Technology,*

*Shenzhen University, Shenzhen 518060, China*

*<sup>5</sup>Institute of Modern Physics, Chinese Academy of Sciences (CAS), Lanzhou 730000, China*

(Dated: August 8, 2018)

## Abstract

**Background:** Fluorine is a key element for nucleosynthetic studies since it is extremely sensitive to the physical conditions within stars. The astrophysical site to produce fluorine is suggested to be asymptotic giant branch (AGB) stars. In these stars the  $^{15}\text{N}(n, \gamma)^{16}\text{N}$  reaction could affect the abundance of fluorine by competing with  $^{15}\text{N}(\alpha, \gamma)^{19}\text{F}$ .

**Purpose:** The  $^{15}\text{N}(n, \gamma)^{16}\text{N}$  reaction rate depends directly on the neutron spectroscopic factors of the low-lying states in  $^{16}\text{N}$ . Shell model calculations and two previous measurements of the  $(d, p)$  reaction yielded the spectroscopic factors with a discrepancy by a factor of  $\sim 2$ . The present work aims to explore these neutron spectroscopic factors through an independent transfer reaction and to determine the stellar rate of the  $^{15}\text{N}(n, \gamma)^{16}\text{N}$  reaction.

**Methods:** The angular distributions of the  $^{15}\text{N}(^7\text{Li}, ^6\text{Li})^{16}\text{N}$  reaction populating the ground state and the first three excited states in  $^{16}\text{N}$  are measured using a Q3D magnetic spectrograph and are used to derive the spectroscopic factors of these states based on distorted wave Born approximation (DWBA) analysis.

**Results:** The spectroscopic factors of these four states are extracted to be  $0.96 \pm 0.09$ ,  $0.69 \pm 0.09$ ,  $0.84 \pm 0.08$  and  $0.65 \pm 0.08$ , respectively. Based on the new spectroscopic factors we derive the  $^{15}\text{N}(n, \gamma)^{16}\text{N}$  reaction rate.

**Conclusions:** The accuracy and precision of the spectroscopic factors are enhanced due to the first application of high-precision magnetic spectrograph for resolving the closely-spaced  $^{16}\text{N}$  levels which can not be achieved in most recent measurement. The present result demonstrates that two levels corresponding to neutron transfers to the  $2s_{1/2}$  orbit in  $^{16}\text{N}$  are not so good single-particle levels although  $^{15}\text{N}$  is a closed neutron-shell nucleus. This finding is contrary to the shell model expectation. The present work also provides an independent examination to shed some light on the existing discrepancies in the spectroscopic factors and the  $^{15}\text{N}(n, \gamma)^{16}\text{N}$  rate.

PACS numbers: 25.60.Je; 25.40.Lw; 26.20.Fj; 27.20.+n

---

\*guobing@ciae.ac.cn

Fluorine ( $^{19}\text{F}$ , the only stable F isotope) is a crucial element for nucleosynthetic studies because it is extremely sensitive to the physical conditions within stars [1]. For a long time, the solar system was the only location of the Galaxy with known fluorine abundance [2]. The astrophysical site to produce fluorine has always been a puzzle. The possible scenario is suggested to be asymptotic giant branch (AGB) stars [3, 4], core-collapse of Type II supernovae [5, 6] and Wolf-Rayet stars [2]. Although the contribution of each source to the F evolution in the Galaxy is still uncertain, the inclusion of all the three sources is necessary to explain the observed Galactic evolution of fluorine [7]. In 1992, spectroscopic observations of giant stars showed enhancements of  $^{19}\text{F}$  by factors of up to 30 with respect to solar abundances, providing the first evidence for  $^{19}\text{F}$  nucleosynthesis in this site [8]. This result has been later supported by the large F enhancements found in post-AGB stars [9] and planetary nebulae [10, 11] which are the progeny of AGB stars. However, AGB model calculations have not yet been able to quantitatively reproduce the highest values of observed  $^{19}\text{F}$  enhancements [4, 12]. Reduction of nuclear reaction rate uncertainties and a better understanding of the nucleosynthesis in the partial mixing zone could help to clarify the discrepancies [12]. A detailed understanding of the nuclear reactions occurring in AGB stars is desirable to simulate fluorine production.

$^{19}\text{F}$  is produced in the He intershell and then dredged up to the surface of AGB stars. The production paths are  $^{14}\text{N}(\alpha, \gamma)^{18}\text{F}(\beta^+)^{18}\text{O}(p, \alpha)^{15}\text{N}(\alpha, \gamma)^{19}\text{F}$  and  $^{14}\text{N}(n, p)^{14}\text{C}(\alpha, \gamma)^{18}\text{O}(p, \alpha)^{15}\text{N}(\alpha, \gamma)^{19}\text{F}$ . Neutrons and protons are liberated by the  $^{13}\text{C}(\alpha, n)^{16}\text{O}$  and  $^{14}\text{N}(n, p)^{14}\text{C}$  reactions, respectively. Furthermore, the neutron- and proton-induced reactions must also be taken into account although  $^{19}\text{F}$  is produced in He-rich environments [12, 13]. The  $^{15}\text{N}(n, \gamma)^{16}\text{N}$  reaction may play an important role in determining the  $^{19}\text{F}$  abundance since it competes with the  $^{15}\text{N}(\alpha, \gamma)^{19}\text{F}$  reaction and removes both neutrons and  $^{15}\text{N}$  from the chain of the  $^{19}\text{F}$  production.

To date considerable work has been performed to study the  $^{15}\text{N}(\alpha, \gamma)^{19}\text{F}$  reaction [14–17]. As for the  $^{15}\text{N}(n, \gamma)^{16}\text{N}$  reaction, only two experimental results [18, 19] were available. In 1996, Meissner et al. [18] measured the  $^{15}\text{N}(n, \gamma)^{16}\text{N}$  cross section at neutron energies of 25 keV, 152 keV, and 370 keV. To interpret the results and calculate the  $^{15}\text{N}(n, \gamma)^{16}\text{N}$  reaction rate, these authors [18] performed direct capture calculations based on the experimental spectroscopic factors of  $^{16}\text{N}$  from measurement of the  $^{15}\text{N}(d, p)^{16}\text{N}$  reaction [20] since the magnitude of the direct capture rate depends directly on the neutron spectroscopic factors of

the four low-lying levels in  $^{16}\text{N}$ . In that work [20] the  $^{15}\text{N}(d, p)^{16}\text{N}$  angular distributions were measured by solid-state detector telescopes with an average energy resolution of 35 keV and yielded nearly equal spectroscopic factors of  $\sim 0.5$  for the ground state and the first three excited states at  $E_x = 0.120$  MeV, 0.298 MeV and 0.397 MeV in  $^{16}\text{N}$ . In 2008, Bardayan et al. [19] measured the angular distributions of the  $^{15}\text{N}(d, p)^{16}\text{N}$  reaction in inverse kinematics by using silicon detector arrays and a recoil separator. Since closely-spaced levels (ground state + 0.120 MeV level, 0.298 + 0.397 MeV levels) could not be resolved, they used two different methods to determine the spectroscopic factors of these four states. The resulting values are larger than the ones in Ref. [20] by a factor of  $\sim 2$ , while are in agreement with shell model expectations [18, 20] where the four low-lying  $^{16}\text{N}$  levels are thought to be good single-particle levels as  $^{15}\text{N}$  is a closed neutron-shell nucleus. Furthermore, they derived the  $^{15}\text{N}(n, \gamma)^{16}\text{N}$  rate via direct capture calculations based on their experimental spectroscopic factors [19]. The updated reaction rate in Ref. [19] is nearly twice faster than the ones in Ref. [18] since the spectroscopic factors used in these two works differ by a factor of  $\sim 2$ .

In short, two previous measurements [19, 20] of the  $(d, p)$  reaction led to the spectroscopic factors with a discrepancy by a factor of  $\sim 2$  and further yielded different  $^{15}\text{N}(n, \gamma)^{16}\text{N}$  rates. Therefore, it is worthwhile to perform a new measurement of the neutron spectroscopic factors for the four low-lying  $^{16}\text{N}$  states via an independent transfer reaction. In this article we report accurate and precision measurement of the spectroscopic factors for these  $^{16}\text{N}$  levels via the angular distribution of the  $^{15}\text{N}(^7\text{Li}, ^6\text{Li})^{16}\text{N}$  reaction using a Q3D magnetic spectrograph. These spectroscopic factors are used to evaluate the  $^{15}\text{N}(n, \gamma)^{16}\text{N}$  reaction rate.

The experiment was performed at the HI-13 tandem accelerator of the China Institute of Atomic Energy (CIAE) in Beijing. The experimental setup and procedures are similar to those previously reported [21–23]. Melamine  $\text{C}_3\text{N}_3(^{15}\text{NH}_2)_3$  enriched to 99.35% in  $^{15}\text{N}$  was employed as target material with a thickness of  $46 \mu\text{g}/\text{cm}^2$ , evaporated on a  $30 \mu\text{g}/\text{cm}^2$  thick carbon foil. To improve thermal conductivity of targets metal gold was evaporated on melamine foil, accumulated to a thickness of  $22 \mu\text{g}/\text{cm}^2$ . The target thickness was determined by using an analytical balance with a precision of  $1 \mu\text{g}$  and was verified with the well-known differential cross sections at  $\theta_{\text{c.m.}} = 33.5^\circ$  and  $49.2^\circ$  of the  $^7\text{Li} + ^{15}\text{N}$  elastic scattering [24, 25]. An uncertainty of 5% was assigned for target thickness, which is reasonable by considering the balance precision and the error of the well-known differential cross

sections.

A 44 MeV  ${}^7\text{Li}$  beam was delivered to measure the angular distribution of the  ${}^{15}\text{N}({}^7\text{Li}, {}^6\text{Li}){}^{16}\text{N}$  reaction leading to the ground state and the first three excited states in  ${}^{16}\text{N}$ . The angular distribution of the  ${}^7\text{Li} + {}^{15}\text{N}$  elastic scattering was also measured to obtain the optical model potential (OMP) for the entrance channel of the transfer reaction. In addition, a 34.5 MeV  ${}^6\text{Li}$  beam was delivered for measurement of the  ${}^6\text{Li} + {}^{15}\text{N}$  elastic scattering to evaluate the OMP for the exit channel.

The beam current was measured by a Faraday cup covering an angular range of  $\pm 6^\circ$  in a laboratory frame and used for the absolute normalization of the cross sections at  $\theta_{\text{lab}} > 6^\circ$ . The Faraday cup was removed when measuring the cross sections at  $\theta_{\text{lab}} \leq 6^\circ$ . A Si  $\Delta E - E$  telescope located at  $\theta_{\text{lab}} = 25^\circ$  was employed for the relative normalization of the cross sections at  $\theta_{\text{lab}} \leq 6^\circ$  by measuring the elastic scattering of the incident ions on the targets. The reaction products were analyzed with a Q3D magnetic spectrograph and recorded by a two-dimensional position-sensitive silicon detector (PSSD,  $50 \times 50$  mm) placed at the focal plane of the spectrograph. The two-dimensional position information from the PSSD enabled the products emitted into the acceptable solid angle to be recorded completely.

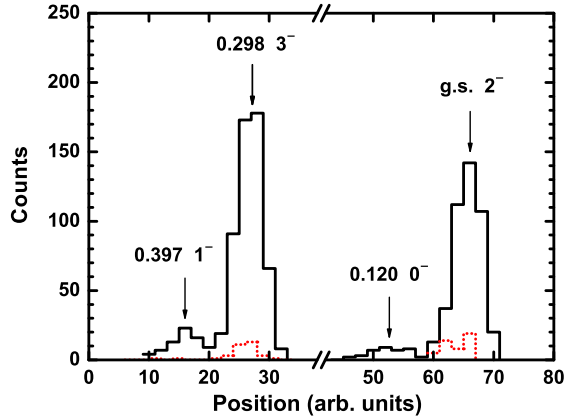


FIG. 1: (Color online) Focal-plane position spectrum of the  ${}^6\text{Li}$  events at  $\theta_{\text{lab}} = 10^\circ$  from the neutron-transfer reactions. The black solid and red dashed lines are the results from the enriched  ${}^{15}\text{N}$  target and natural  ${}^{14}\text{N}$  target, respectively. The break in the x-axis denotes the narrow gap between two separated detectors.

As an example, Fig. 1 shows the focal-plane position spectrum of  ${}^6\text{Li}$  at  $\theta_{\text{lab}} = 10^\circ$  from the

neutron-transfer reactions. The background from  $^{14}\text{N}$  is negligibly small. After background subtraction and beam normalization, the angular distributions of the elastic scattering and the  $^{15}\text{N}(^7\text{Li}, ^6\text{Li})^{16}\text{N}$  reaction leading to the ground and first three excited states in  $^{16}\text{N}$  were obtained, as presented in Figs. 2 and 3.

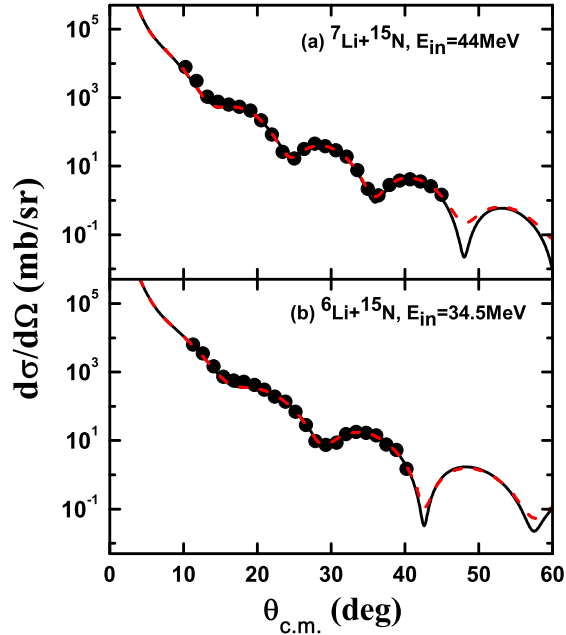


FIG. 2: (Color online) Angular distributions of the  $^7\text{Li}+^{15}\text{N}$  elastic scattering at incident energy of 44 MeV and the  $^6\text{Li}+^{15}\text{N}$  elastic scattering at incident energy of 34.5 MeV. The black solid and red dashed curves represent the calculations using the fitted OMP parameters without and with spin-orbit term, respectively.

The finite-range distorted wave Born approximation (DWBA) method with the FRESKO code [26] was used to analyze the experimental angular distributions. The OMP parameters for the entrance and exit channels were determined by fitting the present experimental angular distributions of the  $^7\text{Li}+^{15}\text{N}$  and  $^6\text{Li}+^{15}\text{N}$  elastic scattering (Fig. 2). The starting values of OMP parameters were obtained by fitting the single-folding nucleus-nucleus potential of Ref. [27]. The real potential was taken to be a squared Woods-Saxon shape, which fits the real part of the folding model potential better than usual Woods-Saxon shape does [28]. For the imaginary potential, Woods-Saxon shape was found to be appropriate. In addition, we investigated the effect of spin-orbit potential parameters although for heavy ions they are thought to have little or no influence on the cross sections [29]. Since the strength

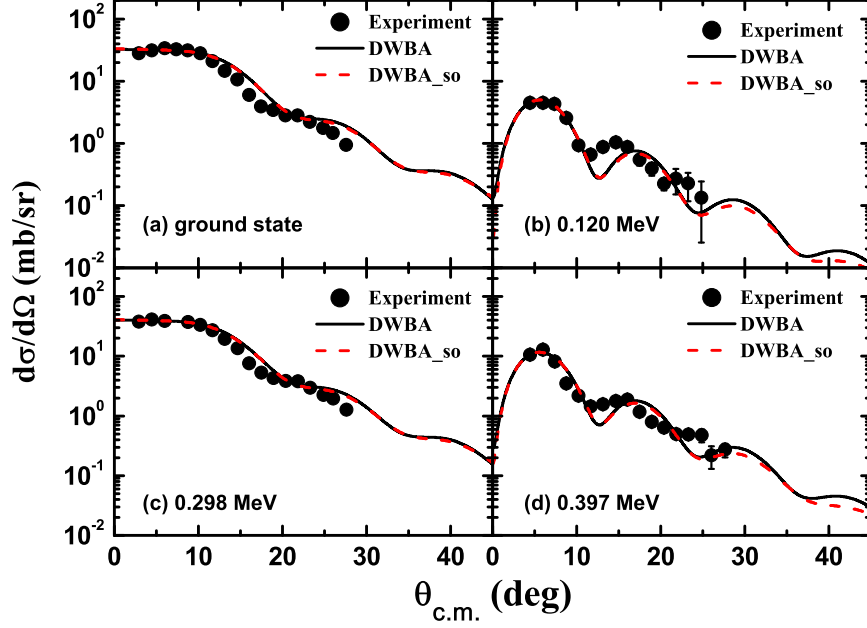


FIG. 3: (Color online) Angular distributions of the  $^{15}\text{N}(^7\text{Li}, ^6\text{Li})^{16}\text{N}$  reaction leading to the ground and first three excited states in  $^{16}\text{N}$ . The black solid and red dashed curves denote the DWBA calculations with the fitted OMP parameters without and with spin-orbit term, respectively.

of the spin-orbit potential for heavy ions scales as  $1/A$  as compared with the nucleon case [29], the depths of the entrance and exit channels were derived to be 0.843 MeV and 0.983 MeV using the depth of 5.9 MeV for nucleon [30]. Both sets of OMP parameters (with and without spin-orbit potential) were used to study spectroscopic factors. Full complex remnant term interactions were included in the transfer reaction calculations. The parameters of the core-core ( $^6\text{Li} + ^{15}\text{N}$ ) potential were obtained using the present ones of  $^6\text{Li} + ^{15}\text{N}$  at 34.5 MeV and systematics in energy dependence of the potential parameters [27]. For the bound state  $^{16}\text{N} = ^{15}\text{N} + n$ , the standard geometrical parameters  $r = 1.25$  fm and  $a = 0.65$  fm were adopted, which have been extensively utilized to study the ground state neutron spectroscopic factors for 80 nuclei of  $Z = 3-24$  [31] and 565 excited state neutron spectroscopic factors for  $Z = 8-28$  nuclei [32]. All the parameters used in the calculation are listed in Table I.

The spectroscopic factors can be derived by the normalization of DWBA calculation to the experimental angular distribution. The neutron spectroscopic factor of the  $^7\text{Li}$  ground state needs to be chosen. So far considerable work has been performed to study it. Shell model

TABLE I: OMP parameters used in the present DWBA calculation.  $E_{\text{in}}$  denotes the incident energy in MeV for the relevant channels,  $V$  and  $W$  are the depths (in MeV) of the real and imaginary potentials with squared Woods-Saxon and usual Woods-Saxon shapes, and  $r$  and  $a$  are the radius and diffuseness (in fm).

| Channel                         | $E_{\text{in}}$ | $V$   | $r_v$ | $a_v$ | $W$  | $r_w$ | $a_w$ | $V_{so}$ | $r_{so}$ | $a_{so}$ | $r_C$ |
|---------------------------------|-----------------|-------|-------|-------|------|-------|-------|----------|----------|----------|-------|
| ${}^7\text{Li}+{}^{15}\text{N}$ | 44.0            | 138.7 | 0.911 | 1.26  | 45.0 | 0.966 | 0.820 |          |          |          | 1.30  |
|                                 |                 | 118.9 | 0.899 | 1.36  | 49.3 | 0.923 | 0.795 | 0.843    | 0.974    | 1.36     | 1.30  |
| ${}^6\text{Li}+{}^{16}\text{N}$ | 34.5            | 111.0 | 0.886 | 1.47  | 39.0 | 0.840 | 1.02  |          |          |          | 1.30  |
|                                 |                 | 91.0  | 0.930 | 1.43  | 29.3 | 0.841 | 1.12  | 0.983    | 0.786    | 1.37     | 1.30  |
| ${}^6\text{Li}+{}^{15}\text{N}$ | 37.7            | 132.0 | 0.901 | 1.37  | 31.3 | 0.945 | 0.918 |          |          |          | 1.30  |
| $n+{}^{15}\text{N}$             |                 | $a$   | 1.25  | 0.65  |      |       |       | 6.0      | 1.25     | 0.65     | 1.25  |

<sup>a</sup>The depth was obtained by fitting to reproduce the binding energy of the neutron in  ${}^{16}\text{N}$ .

calculations [33–36] predicted values of 0.80, 0.72, 0.79 and 0.77. Three measurements [37–39] of the  ${}^7\text{Li}(p, d)$  reaction yielded consistent spectroscopic factors of 0.71, 0.72 and 0.87. However, two measurements [31, 40] of the  ${}^6\text{Li}(d, p)$  reaction derived very different values of 0.9 and 1.85. In addition, most recent measurement of the elastic-transfer  ${}^7\text{Li}({}^6\text{Li}, {}^7\text{Li})$  reaction yielded a value of 0.73 [41]. In view of these different evaluations, we decided to use the value of 0.73 [34, 37, 38, 41]. The  $1p_{3/2}$  and  $1p_{1/2}$  components in the spectroscopic factor of  ${}^7\text{Li}$  were taken to be 1.5 based on the shell model calculation [34]. The spectroscopic factors of the ground state and the first three excited states in  ${}^{16}\text{N}$  were then extracted to be  $0.96 \pm 0.09$ ,  $0.69 \pm 0.09$ ,  $0.84 \pm 0.08$  and  $0.65 \pm 0.08$ , respectively. The errors result from the statistics (8%, 12%, 8%, 11%), the uncertainty of target thickness (5%) and the OMP parameters (1.6%, 2.2%, 1.2%, 3.1%), respectively. Additional model uncertainties were not included when evaluating the uncertainty of spectroscopic factors, as two previous work [19, 20] did. In this work we also tested the effect of changing the geometrical parameters of the binding potential on spectroscopic factors. We changed the radius and diffuseness 20% around the standard values ( $r = 1.25$  fm,  $a = 0.65$  fm), and then found that the spectroscopic factors of the two states corresponding to  $1d_{5/2}$  transfer vary by  $\sim 20\%$  and those of the two states corresponding to  $2s_{1/2}$  transfer vary by  $\sim 8\%$ . This difference in response to transfers to the  $1d_{5/2}$  and  $2s_{1/2}$  states may come from the different peripheralities of these



TABLE II: The present spectroscopic factors of  $^{16}\text{N}$  and other available results in the literature.  $nl_j$  is single-particle shell quantum number.

| $E_x$<br>(MeV) | $J^\pi$ | $nl_j$     | Spectroscopic factor |   |                                     |                      |         |
|----------------|---------|------------|----------------------|---|-------------------------------------|----------------------|---------|
|                |         |            | OXBASH [18]          | $^{15}\text{N}(d, p)$ [20] <sup>a</sup> | $^2\text{H}(^{15}\text{N}, p)$ [19] | Present              |         |
|                |         |            |                      |   | Method1 <sup>b</sup>                | Method2 <sup>c</sup> |         |
| 0              | $2^-$   | $1d_{5/2}$ | 0.93                 | 0.55                                    | 0.96(15)                            | 1.04(16)             | 0.96(9) |
| 0.120          | $0^-$   | $2s_{1/2}$ | 0.95                 | 0.46                                    | 0.80(12)                            | 0.71(12)             | 0.69(9) |
| 0.298          | $3^-$   | $1d_{5/2}$ | 0.87                 | 0.54                                    | 0.91(14)                            | 1.03(16)             | 0.84(8) |
| 0.397          | $1^-$   | $2s_{1/2}$ | 0.96                 | 0.52                                    | 0.88(13)                            | 0.74(12)             | 0.65(8) |

<sup>a</sup>30% uncertainty for their spectroscopic factors.

<sup>b</sup>The individual components were weighted by the relative spectroscopic factors reported in Ref. [20].

<sup>c</sup>The magnitudes of the individual components were allowed to vary freely in fit.

two transitions.

The new spectroscopic factors are listed in Table II, together with the ones from two previous measurements of the  $^{15}\text{N}(d, p)$  reaction [19, 20] and the shell model calculation [18]. The present results are approximately twice larger than those from the  $^{15}\text{N}(d, p)$  reaction [20], while are in good agreement with those from the  $^2\text{H}(^{15}\text{N}, p)$  reaction using Method2 (namely, components allowed to vary freely) in Ref. [19] where two different methods were used to determine the spectroscopic factors since closely-spaced levels (ground state + 0.120 MeV level, 0.298 + 0.397 MeV levels) in  $^{16}\text{N}$  could not be resolved. The present results demonstrate that two levels corresponding to neutron transfers to the  $1d_{5/2}$  orbit in  $^{16}\text{N}$  are good single-particle levels but two levels corresponding to neutron transfers to the  $2s_{1/2}$  orbit are not so good single-particle levels as the shell model expected [18].

We computed the direct capture cross section and the rate of  $^{15}\text{N}(n, \gamma)^{16}\text{N}$  based on the measured spectroscopic factors using the RADCAP code [42]. At low energies of astrophysical interest, the  $^{15}\text{N}(n, \gamma)^{16}\text{N}$  direct capture cross section is dominated by the  $E1$  transition from incoming  $p$ -wave to the bound state. Note that the same geometrical parameters need to be used when calculating the bound state wave function as those used for deriving the spectroscopic factors of  $^{16}\text{N}$ . In addition, the parameters for computing the scattering wave

function are identical to the ones for the bound state potential, as suggested by Huang et al. [43]. We also evaluated the contribution of the resonant capture via the state at  $E_x = 3.523$  MeV using the resonance parameters given by Meissner et al. [18]. The resulting rates are shown in Fig. 4(a). The rate is dominated by the direct capture at temperatures of  $T_9 < 2$ . The total reaction rate at  $T_9 = 0.1$  (typical temperature of AGB stars) was found to be  $504 \pm 66 \text{ cm}^3 \text{ mol}^{-1} \text{ s}^{-1}$ , The error results from the uncertainty (12%) of the present spectroscopic factors and that (5.3%) of the geometrical parameters.

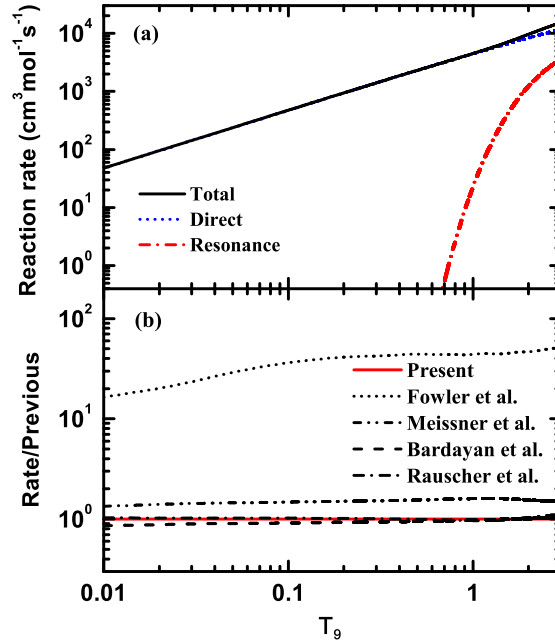


FIG. 4: (Color online) The present  $^{15}\text{N}(n, \gamma)^{16}\text{N}$  rate for temperatures of 0.01-3 GK, and comparison of the present rate with the previous results by Fowler et al. [44], Rauscher et al. [45], Meissner et al. [18] and Bardayan et al. [19].  $T_9$  is the temperature in units of 1 GK. See text for details.

In Fig. 4(b) we compare the present rate with the previous ones available in the literature [18, 19, 44, 45]. The present rate is about 20-50 times faster than the previous calculation [44] since it is a first order estimate of the  $p$ -wave capture contribution. The present rate is also nearly twice faster than the experimental ones in Ref. [18]. This is because the present spectroscopic factors are larger than the ones from the  $^{15}\text{N}(d, p)$  reaction [20] used in Ref. [18]. In addition, the new rate within 10% agrees with the ones in Refs. [19, 45] since the new spectroscopic factors are consistent with those from the shell model calculation [45] and

the  ${}^2\text{H}({}^{15}\text{N}, p)$  reaction [19].

The new rate was fitted with the expression used in the astrophysical reaction rate library REACLIB [46],

$$N_A \langle \sigma v \rangle = \exp[6.38075 + 0.0159372T_9^{-1} - 1.80122T_9^{-1/3} + 4.02273T_9^{1/3} - 0.108521T_9 - 0.0221989T_9^{5/3} - 0.754253 \ln(T_9)]. \quad (1)$$

The overall fitting errors are less than 6% at temperatures from 0.01 to 10 GK.

In summary, the angular distributions of the  ${}^{15}\text{N}({}^7\text{Li}, {}^6\text{Li}){}^{16}\text{N}$  reaction leading to the four low-lying  ${}^{16}\text{N}$  levels were measured and used to derive their spectroscopic factors. The closely-spaced levels in  ${}^{16}\text{N}$  were resolved and the accuracy and precision of spectroscopic factors are enhanced due to the first application of high-precision magnetic spectrograph for study of the neutron transfer reaction on  ${}^{15}\text{N}$ . The present work demonstrates that two levels corresponding to neutron transfers to the  $1d_{5/2}$  orbit in  ${}^{16}\text{N}$  are good single-particle levels but two levels corresponding to neutron transfers to the  $2s_{1/2}$  orbit are not so good single-particle levels as the shell model expected [18].

We also derived the  ${}^{15}\text{N}(n, \gamma){}^{16}\text{N}$  reaction rate using the measured spectroscopic factors. The present rate is about 20-50 times faster than the previous calculation [44] and is nearly twice faster than the experimental ones in Ref. [18]. In addition, the new rate is within 10% in agreement with the ones in Refs. [19, 45]. The present work provides an independent examination to shed some light on the existing discrepancies in the spectroscopic factors of the four low-lying  ${}^{16}\text{N}$  states and the stellar rate of the  ${}^{15}\text{N}(n, \gamma){}^{16}\text{N}$  reaction.

The authors thank the staff of HI-13 tandem accelerator for the smooth operation of the machine, R. C. Johnson and N. K. Timofeyuk for their helpful discussions. We acknowledge the anonymous referee for helpful comments and suggestions. This work was supported by the National Natural Science Foundation of China under Grant Nos. 11075219, 11321064, 11375269, 11275272 and 11275018, the 973 program of China under Grant No. 2013CB834406.

---

[1] S. Lucatello, T. Masseron, J. A. Johnson et al., *Astrophys. J.* **729**, 40 (2011).

[2] G. Meynet and M. Arnould, *Astron. Astrophys.* **355**, 176 (2000).

- [3] M. Forestini, S. Goriely, A. Jorissen et al., *Astron. Astrophys.* **261**, 157 (1992).
- [4] S. Cristallo, O. Straniero, R. Gallino et al. *Astrophys. J.* **696**, 797 (2009).
- [5] S. E. Woosley, D. H. Hartmann, R. D. Hoffman et al., *Astrophys. J.* **356**, 272 (1990).
- [6] S. E. Woosley, A. Heger and T. A. Weaver, *Rev. Mod. Phys.* **74**, 1015 (2002).
- [7] A. Renda, Y. Fenner, B. K. Gibson et al., *Mon. Not. R. Astron. Soc.* **354**, 575 (2004).
- [8] A. Jorissen, V. V. Smith and D. L. Lambert, *Astron. Astrophys.* **261**, 164 (1992).
- [9] K. Werner, T. Rauch and J. W. Kruk, *Astron. Astrophys.* **433**, 641 (2005).
- [10] Y. Zhang and X. W. Liu, *Astrophys. J.* **631**, L61 (2005).
- [11] M. Otsuka, H. Izumiura, A. Tajitsu and S. Hyung, *Astrophys. J.* **682**, L105 (2008).
- [12] M. Lugaro, C. Ugalde, A. I. Karakas et al., *Astrophys. J.* **615**, 934 (2004).
- [13] F. Herwig, N. Langer, M. Lugaro, *Astrophys. J.* **593**, 1056 (2003).
- [14] F. de Oliveira, A. Coc, P. Aguer et al., *Phys. Rev. C* **55**, 3149 (1997).
- [15] S. Wilmes, V. Wilmes, G. Staudt, P. Mohr and J. W. Hammer, *Phys. Rev. C* **66**, 065802 (2002).
- [16] H. T. Fortune and A. G. Lacaze, *Phys. Rev. C* **67**, 064305 (2003).
- [17] K. E. Rehm, *J. Phys. Conf. Ser.* **337**, 012006 (2012).
- [18] J. Meissner, H. Schatz, H. Herndl et al., *Phys. Rev. C* **53**, 977 (1996).
- [19] D. W. Bardayan, P. D. O'Malley, J. C. Blackmon et al., *Phys. Rev. C* **78**, 052801R (2008).
- [20] W. Bohne, J. Bommer, H. Fuchs et al., *Nucl. Phys. A* **196**, 41 (1972).
- [21] B. Guo, Z. H. Li, M. Lugaro et al., *Astrophys. J.* **756**, 193 (2012).
- [22] Y. J. Li, Z. H. Li, E. T. Li et al., *Eur. Phys. J. A* **48**, 13 (2012).
- [23] Z. H. Li, Y. J. Li, J. Su et al., *Phys. Rev. C* **87**, 017601 (2013).
- [24] C. L. Woods, B. A. Brown and N. A. Jelley, *J. Phys. G* **8**, 1699 (1982).
- [25] F. de Oliveira, A. Coc, P. Aguer et al., *Nucl. Phys. A* **597**, 231 (1996).
- [26] I. J. Thompson, *Comput. Phys. Rep.* **7**, 167 (1988).
- [27] Y. P. Xu and D. Y. Pang, *Phys. Rev. C* **87**, 044605 (2013).
- [28] D. T. Khoa, W. V. Oertzen, H. G. Bohlen and S. Ohkubo, *J. Phys. G* **34**, R111 (2007).
- [29] L. Trache, A. Azhari, H. L. Clark et al., *Phys. Rev. C* **61**, 024612 (2000).
- [30] R. L. Varner, W. J. Thompson, T. L. McAbee et al., *Phys. Rep.* **201**, 57 (1991).
- [31] M. B. Tsang, J. Lee and W. G. Lynch, *Phys. Rev. Lett.* **95**, 222501 (2005).
- [32] M. B. Tsang, J. Lee, S. C. Su et al., *Phys. Rev. Lett.* **102**, 062501 (2009).

- [33] F. C. Barker, Nucl. Phys. A **83**, 418 (1966).
- [34] S. Cohen and D. Kurath, Nucl. Phys. A **101**, 1 (1967).
- [35] S. Varma and P. Goldhammer, Nucl. Phys. A **125**, 193 (1969).
- [36] N. Kumar, Nucl. Phys. A **225**, 221 (1974).
- [37] T. Y. Li and S. K. Mark, Nucl. Phys. A **123**, 147 (1969).
- [38] I. S. Towner, Nucl. Phys. A **126**, 97 (1969).
- [39] B. Fagerström et al, Phys. Scr. **13**, 101 (1976).
- [40] J. P. Schiffer, G. C. Morrison, R. H. Siemssen et al. Phys. Rev. **164**, 1274 (1967).
- [41] J. Su, Z. H. Li, B. Guo et al., Chin. Phys. Lett. **27**, 052101 (2010).
- [42] C. A. Bertulani, Comput. Phys. Commun. **156**, 123 (2003).
- [43] J. T. Huang, C. A. Bertulani and V. Guimarães, At. Data Nucl. Data Tables **96**, 824 (2010).
- [44] W. A. Fowler, G. E. Caughlin and B. A. Zimmerman, Annu. Rev. Astron. Astrophys. **5**, 525 (1967).
- [45] T. Rauscher, J. H. Applegate, J. J. Cowan et al., Astrophys. J. **429**, 499 (1994).
- [46] F.-K. Thielemann, M. Arnould and J. Truran, in Advances in Nuclear Astrophysics, ed. A. Vangioni-Flam (Gif-sur-Yvette: Editions Frontière), 525 (1987).